The AXAF High Resolution Camera(HRC): Calibration and Recalibration at XRCF and Beyond

S. S. Murray[a], J. H. Chappell[a], A. T. Kenter[a], K. Kobayashi[a], R. P. Kraft[a],
G. R. Meehan[a], M. V. Zombeck[a], G. W. Fraser[b],
J. F. Pearson[b], J. E. Lees[b], A. N. Brunton[b],
S. E. Pearce[b], M. Barbera[c], A. Collura[c],
S. Serio[c]

[a]Smithsonian Institution Astrophysical Observatory
High Energy Astrophysics Division
60 Garden Street
Cambridge, MA 02138 USA

[b]University of Leicester
Department of Physics and Astronomy
University Road
Leicester, LE1 7RH England

[c]Instituto e Osservatario Astronomico G. S. Vaiana
Palazzo dei Normanni
90134 Palermo Italy

ABSTRACT

The High Resolution Camera (HRC) is a Microchannel Plate based imaging detector for the Advanced X-Ray Astrophysics Facility (AXAF) that will be placed in a high earth orbit scheduled for launch in August, 1998. An end-to-end calibration of the HRC and the AXAF High Resolution Mirror Assembly (HRMA) was carried out at the Marshall Space Flight Center's X-Ray Calibration Facility (XRCF). This activity was followed by several modifications to the HRC to improve its performance, and a series of flat field calibrations. In this paper, and the following companion papers, we discuss the calibration plans, sequences, and results of these tests. At the time of this conference, the HRC has been fully flight qualified and is being integrated into the Science Instrument Module (SIM) in preparation for integration into the AXAF spacecraft.

Keywords: X-ray detectors, calibration, flat field, microchannel plate
High Resolution Camera, AXAF

1. INTRODUCTION

The High Resolution Camera (HRC) is one of two focal plane instruments that will soon be launched on the Advanced X-Ray Astrophysics Facility (AXAF). Construction of the Flight Unit was completed in early 1997 and the instrument was shipped to the X-Ray Calibration Facility (XRCF) at NASA's Marshall Space Flight Center on 23 February, 1997 for end-to-end calibration with the High Resolution Mirror Assembly (HRMA). This paper briefly reviews the design of the HRC, outlines the calibration plan for the XRCF, summarizes the qualitative results from the XRCF, describes the modifications made to the Flight Unit, and illustrates the results of these improvements. Details with regard to the final performance measurements of the HRC are given in companion papers presented at this session[1,2,3].

2. HRC DESCRIPTION

The HRC consists of two detector units packaged in a common housing and sharing event processing electronics. The focal plane layout is shown in Figure 1. Much of the detail regarding the HRC has been presented previously and will not be repeated here [4].

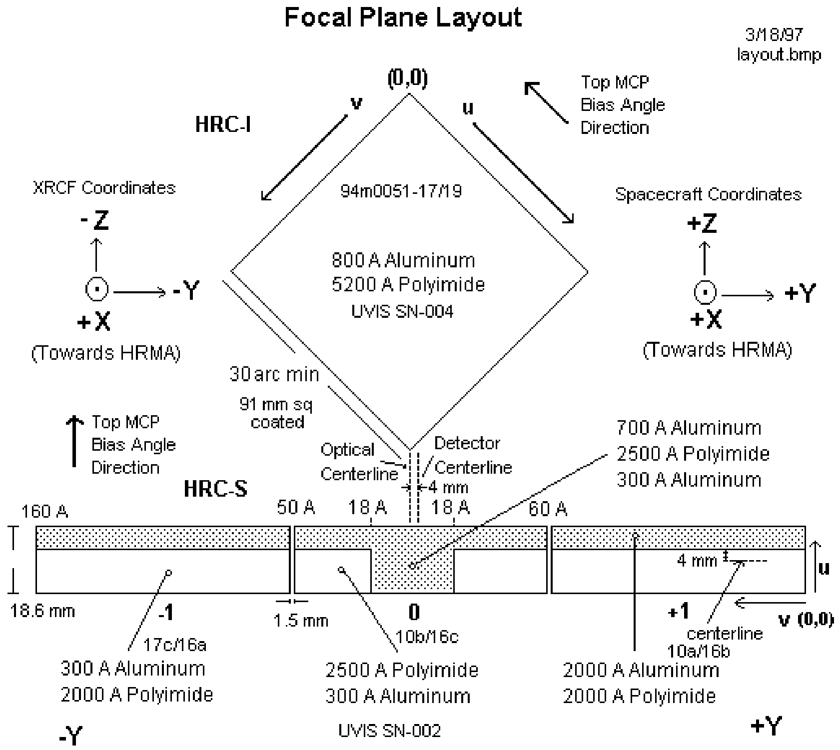

Figure 1. Layout of the HRC focal plan as viewed looking into the detector housing from the telescope.

The square MCP detector (HRC-I) has been optimized for direct x-ray imaging. Its large field of view (1/2° on a side) and extremely low background will permit high sensitivity deep exposures to be taken. The internal HRC background measured during the XRCF tests was well below 0.1 $ct\ cm^{-2}sec^{-1}$, a result of the use of low background MCP's manufactured using radioactive isotope free glass. The AXAF plate scale of $50\mu m\ arcsecond^{-1}$ (10m focal length), and the high quality of the telescope (about 0.5 arc-second FWHM) allow source detection to be carried out using arc-second cell sizes. The non-x-ray background in a 1 arc-second pixel is of the order 1 count per fortnight (i.e., about 1 $ct\ arcsecond^{-2}$ per $10^6 seconds$).

The HRC-I can also be used as a readout device for the High Energy Transmission Grating Spectrometer (HETGS)[5] that disperses X-rays along the diagonal of the detector. This mode of operation serves as a backup to the primary HETGS readout, the spectroscopy array of CCD's that are part of the AXAF Imaging CCD Spectrometer (ACIS).

The long segmented MCP detector (HRC-S) has been optimized for reading out the Low Energy Transmission Grating Spectrometer (LETGS)[6] that disperses X-rays according to their energy along the Y-axis of the spacecraft (which corresponds to the long axis of the HRC-S). The internal background of this detector is very low, comparable to the HRC-I, and long exposure times are possible without significant background contributions.

The HRC-S includes two features that improve its performance as a grating read out. As shown in Figure 1, the UV Ion Shield (UVIS) has a pattern of various thicknesses of Aluminum overcoating. In the central region of the HRC-S the thicker Aluminum blocks FUV and EUV well enough to allow direct imaging as a backup to the HRC-I, albeit over a smaller field of view. The long thin strip of high Aluminization along one edge of the three segments can be used to block low energy x-rays from first order diffraction by the LETGS. This enhances the relative strength of the higher order spectrum compared with those in first order, useful for taking advantage of the greater spectral resolution of these higher orders.

The second feature included with the HRC-S, is the inclusion of a pair of reflecting flats that can intercept the incoming x-ray beam. These reflectors are shown in Figure 2. They are made of polished Nickel Kanigen on

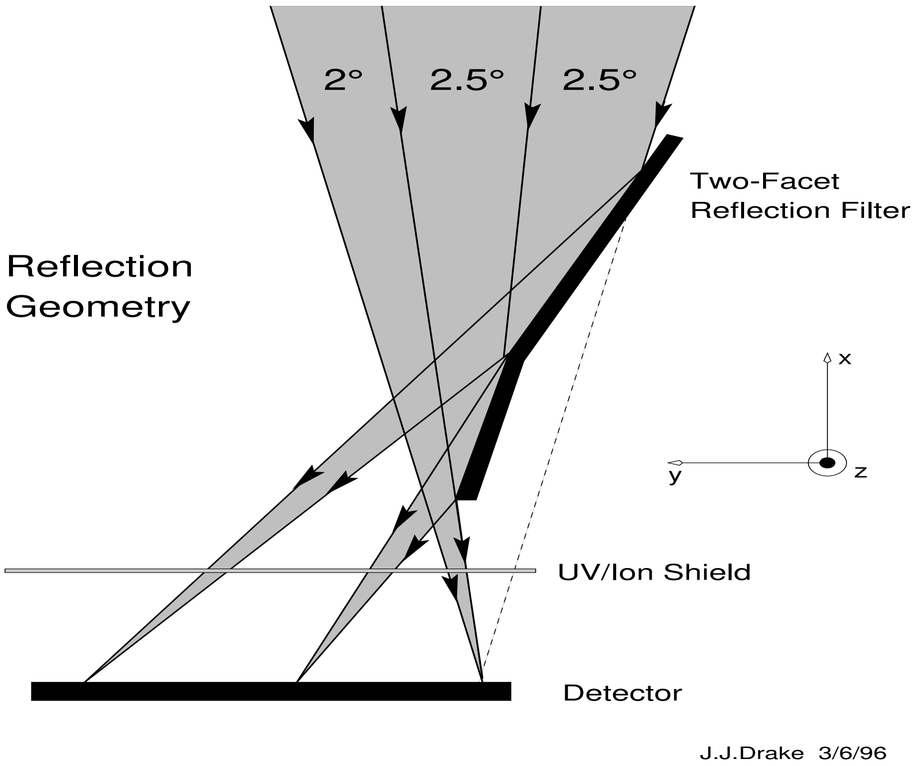

Figure 2. The High Energy Suppression Filter. The converging cone of X-rays from the telescope reflects off the coated flats for low energies, and is absorbed at high energies. The resulting image consists of three components, one from each of the two facets, and one from the direct image.

Beryllium substrates, that are then over coated with Carbon or Chromium. At a grazing incidence of a few degrees the reflectivity of these materials cuts off at about 0.5 keV, thus preferentially blocking the high energy x-rays from being detected. As a result, the first order spectra from the LETGS are enhanced relative to the higher orders that would otherwise overlap on the detector. Although the High Energy Suppression Filter (HESF) was a late addition to the detector design, it was included in the instrument when calibrated at the XRCF. We are still analyzing the data from that portion of the calibration. However, it is clear from the quick look analysis that the flats are properly installed and functioning.

3. CALIBRATION

3.1. Subsystem Calibration at SAO

Calibration of the HRC began with subsystem level measurements of the detector components. Uncoated MCP's were screened and flat fielded at Al-K (1.5keV) prior to selection for flight. After coating with CsI, the absolute efficiency was measured at 8 energies using a multi-anode Manson electron impact source to generate characteristic x-ray lines, and flow proportional counters as a flux monitor. Flat fields were also obtained at these energies. Sufficient counts were collected to give at least 3% statistical precision on a 0.8x0.8 mm^2 scale. Figure 3 shows the quantum efficiency measurements for the HRC-I obtained in this calibration. Details of this phase of the calibration were reported at the previous SPITE conference. It is remarkable that these efficiencies are virtually the same as those estimated in the original HRC proposal of 1984.

Uniformity and transmission of the UVIS's were measured using a non-flight HRC and taking the difference between images with the filters in and out of the beam. We also measured the absolute transmission of witness samples of the windows using an X-ray fluorescence source (X-Kit). Results from this phase of the work have also been reported at previous SPIE conferences[7].

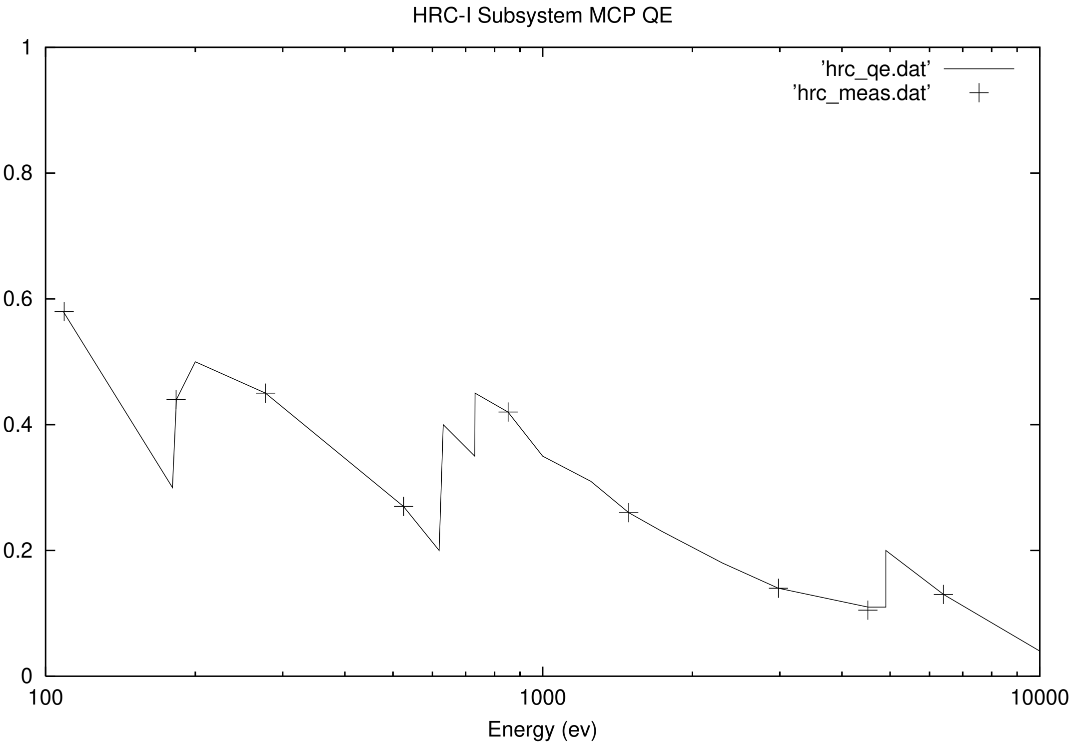

Figure 3. HRC-I quantum efficiency measured at subsystem level at SAO prior to detector housing assembly. The solid line is a coarse model of the efficiency versus energy taking into account only major absorption edges.

3.2. Flight Calibration at XRCF

When the detector housing was fully assembled, verification measurements were made to confirm that the completed unit was working properly. Overall absolute efficiency for the HRC was measured at the same 8 energies used previously. During this time period, the flight UVIS's were damaged and replaced. Unfortunately, there was no time to completely calibrate the replacement filters to the same level as the original flight items. However, the comprehensive witness sample program has allowed us to confidently infer the replacement filter characteristics as will be reported during this session[3]. We found no significant changes in the detector efficiency nor any significant spatial non-uniformities.

Following these subsystem calibrations and full assembly verification tests, the HRC was shipped to MSFC for further calibration with the AXAF X-ray telescope. The majority of the tests planned were measurements of the overall effective area (telescope plus detector) at numerous energies. One of the features of the XRCF is the X-ray Source System (XSS) which includes a Double Crystal Monochrometer source (DCM) and a High Resolution Erect Field Spectrometer source (HIREF). These sources provided "dial-up" energy selection allowing us to examine the system performance near known features (e.g. absorption edges in the UVIS, MCP, and CsI coating) as well as in regions well away from such features. With the presence of the HRMA, it was also possible to measure the effects of a converging beam on to the MCP pores in the same geometry as for flight (to be compared with laboratory tests using collimated beams) and the the reflectivity of the HESF mirrors at the same angles as in flight. Other tests involved measuring the count rate linearity of the detectors, the spatial linearity over large and small scales, and verifying the point response function of the total system on and off axis.

The availability of the transmission grating spectrometers at the XRCF also provided an opportunity for calibrating the performance of the HRC-S/LETGS and HRC-I/HETGS. These tests were included in the overall calibration plan at XRCF. They were mainly measurements of total effective area for the combined instruments, and measurements of the point spread function convolved with the grating response to obtain the energy resolution of the

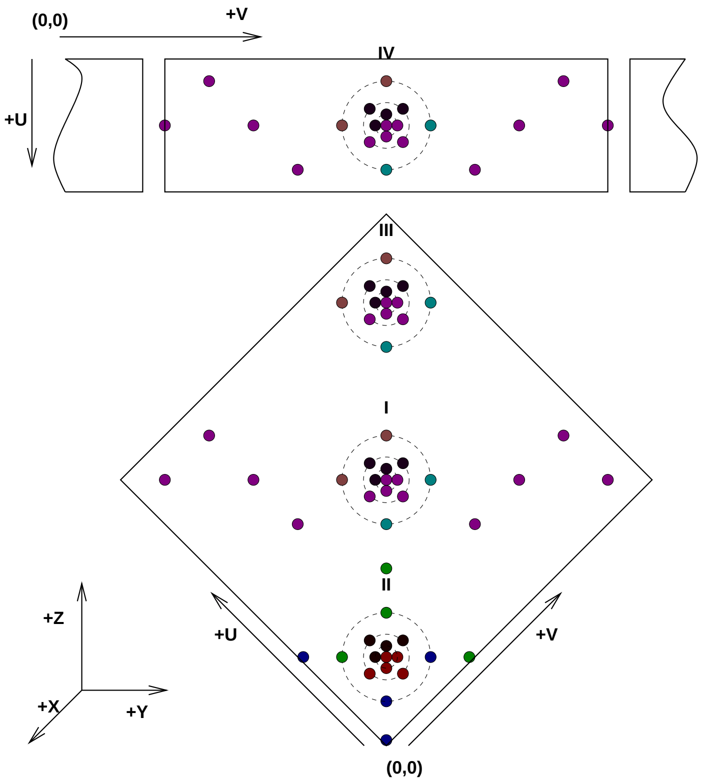

Figure 4. Aim points on the HRC as it appears at XRCF looking from the telescope towards the focal plane. The dots are locations where the image of the point source may be located during the calibration. Each detector has a local coordinate system corresponding to the EGSE display system - these are labeled U,V. The facility coordinate system is indicated as X,Y,Z (this is NOT the spacecraft system). The pattern of aim points allows on-axis and off-axis measurements sampling different regions of the the detector and different azimuths.

spectrometers. The primary analysis of these data is being carried out by the Grating teams.

Since two detectors were being calibrated as well as two spectrometers, the number of individual tests quickly became large. Each test is characterized by many parameters - the source configuration, the geometry of the X-ray telescope and HRC, the grating status, and the configuration of the various beam monitors. To manage these tests and generate a test sequence, a Calibration Master Data Base (CMDB) was created by the AXAF Science Center, and scheduling software was written to maximize the total throughput of the system. Sustained 24 hour a day, seven day a week operation was required to complete the calibration program within the allowed time, which for HRC plus LETGS was just 24 days of beam time. In that time we successfully completed the entire planned program as well as numerous added tests, for a total of 1111 measurements. The overall testing efficiency achieved in this phase of the XRCF very good. We were collecting data for about 70% of real time over the time period 19 March, 1997 to 12, April 1997.

Figure 4 shows the locations of aim points on the HRC for the XRCF. Due to the count life restrictions of an MCP detector, we were very careful to avoid long X-ray exposure at any single location of the detector. In many cases this was achieved by deliberately positioning the HRC slightly out of focus and spreading out the incident flux. This strategy was well suited for effective area measurements since our flat field data showed that the detector does not have large variations in response on the scale of about a millimeter. In actual observations, the AXAF spacecraft will be slowly dithered in a 2-D pattern with about a 1 millimeter amplitude averaging out small scale variations, and avoiding high exposure to any single MCP pore.

The first light x-ray image for the HRC in the XRCF was obtained using the HRC-I and with the detector located about 25 mm in front of the focal plane. This image is shown in Figure 5. Two out of 16 mirror shutters were closed

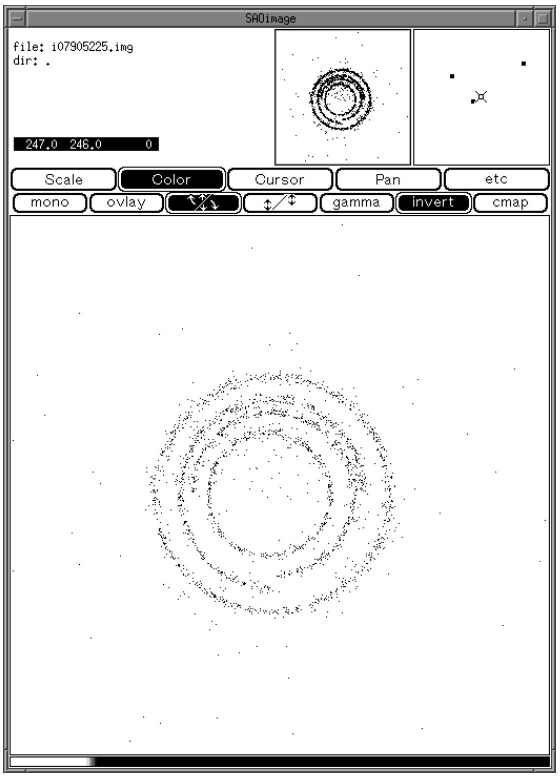

Figure 5. The first X-ray image at XRCF using the HRC-I. The detector is situated about 25 mm in front of the focal plane, with two quadrant shutters closed on shells 3 and 4 of the HRMA.

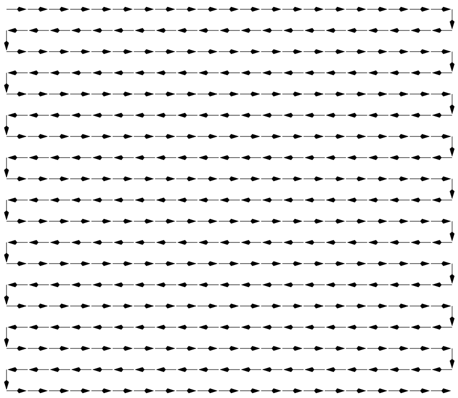

Figure 6. Typical serpentine "dither" pattern used at XRCF to simulate the spacecraft motion and to avoid over exposure on the HRC.

during this test, one each on HRMA shells 3 and 4 in order to verify the orientation of the HRC UV plane with respect to the calibration facility, and to confirm that the detector was properly located in the axial (X) direction.

For those cases where defocus was not an option (e.g. measurement of the point spread function or grating resolution), we used a simulated dither mode by moving the detector in the Y-Z plane in small steps for small time intervals. A typical "dither" consisted of a serpentine pattern of $40\mu m$ steps every 5 seconds, first in the Y-axis and then in the Z-axis (see Figure 6). In the data analysis, these motions can be "taken out" in the same manner as an aspect correction made to the detected coordinates of each photon.

Figure 7a shows an uncorrected image taken while dithering in a $800\mu m$ box. The HRC-I detector is rotated

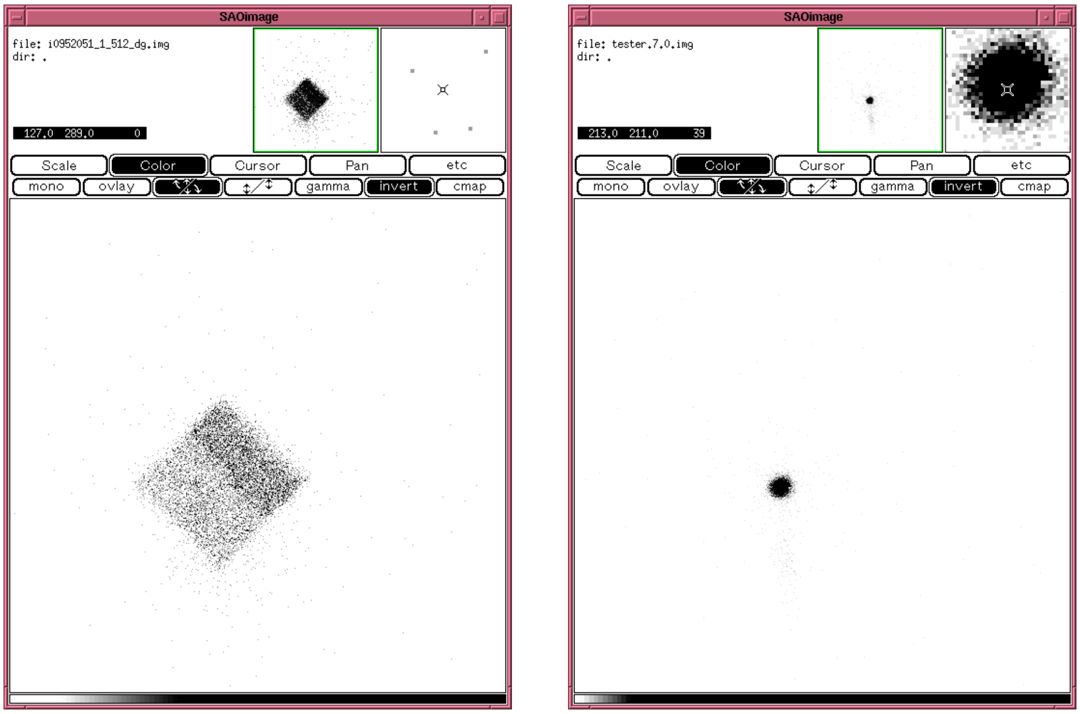

(a) Uncorrected "dithered" image **(b) Corrected image**

Figure 7. An HRC-I image taken at XRCF while dithering to avoid over exposure of the MCP. The test was made using the C-K EIPS source, and the HRC was place at the focus of the telescope. (a) is the uncorrected image,(b) is the image after correcting for the FAM motion.

approximately 45° relative to the facility. In Figure 7b, the corrected image is shown. The corrections were made by selecting out X-ray events that occurred only when the detector was not moving and re-mapping those photon positions by the offset of the detector from a nominal reference position. Time tagging for each detected event is a part of the HRC data structure. An independent time tag is provided for the focal plane mount that holds the HRC. This assembly, provided by Ball Aerospace, consists of a Simulated Science Instrument Module (LASSZ), and a movable table (the FAM) which can move in X,Y,Z in $10\mu m$ steps and also can rotate about each axis (θ_x, θ_y, θ_z). The HRC and FAM clocks are referenced to IRIG-B (Inter-Range Instrumentation Group) time generators for synchronization.

In Figure 8 we show the energies at which effective area measurements were made for the HRC-I. For reference, the plot shows shows a smooth curve of QE versus energy with little or no detail at the locations of expected features due to absorption. The vertical lines show the energies at which we measured the effective area. These bracket expected features (shown as points) so that any jumps can be measured. We also included intermediate energies to constrain the curve in featureless regions. In all, approximately 50 energies were selected spanning the 0.1 to 10 keV region of the spectrum. With the exception of a few electron impact source lines (e.g. B-K, Be-K, C-K), these energies were achieved with the DCM and HIREFS sources.

3.3. Annomolous Behavior - Oops!

Following the tests using the mirror and gratings, we had planned to conduct a series of flat field exposures at the XRCF taking advantage of the very uniform beam (due to the long distance from the source to the detector), and the excellent ancillary beam monitoring equipment. However, these tests were not carried out at the XRCF.

3.3.1. Ripple

Prior to the start of the XRCF tests, the HRC was baked out in a special MSFC facility to make sure that the instrument would not contaminate the HRMA. During the bakeout test, we were able to operate the fully assembled

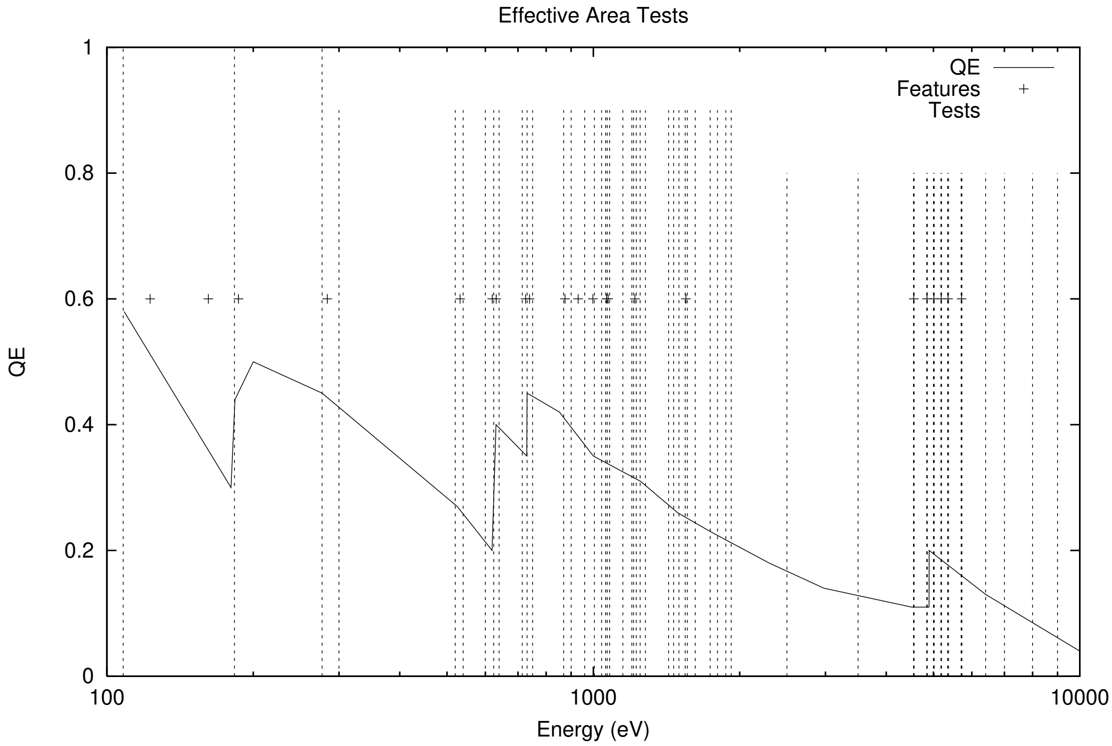

Figure 8. Plot of the approximate QE versus Energy for the HRC-I detector. The "pluses" indicate energies where a feature is expected in a detailed plot, usually due to some absorption edge in the materials of the UVIS, MCP, or coating. The lines show the energies that were planned for measurement at the XRCF.

system for the first time. In these tests we noted a large number of event trigger signals with no valid readout signal. We were we able to access only a few test points on the detector in the bakeout facility and examined some of the readout signals. We discovered a 91 KHz noise signal that was only present when MCP high voltage was turned on. The amplitude of the noise correlated with the high voltage value. Although we could not monitor the event trigger signal directly, we concluded that this 91 KHz noise was also present on the MCP trigger signal, resulting in the large number of false events.

A quick remedy was to change the threshold level for event triggers. This level is commandable and it was raised to eliminate the false triggers. Specifically, the HRC-I threshold was raised from about 10 DU to 32 DU (out of a maximum of 255), and the HRC-S threshold was increased from about 10 DU to 40 DU. Post XRCF tests showed that the HRC-I threshold setting could have been as low as about 20 DU while still eliminating most false triggers. At the time, this seemed to be a minor change in the operation of the HRC, as the threshold was only changed by the equivalent of a few percent of its adjustment range. In retrospect, this resulted in a significant change in performance (as discussed below).

3.3.2. High Gain

When the HRC was finally installed in the XRCF and we began the the test sequence with X-rays through the telescope, we noted that a large fraction of detected events had total pulse heights at the saturation limit of the readout electronics. As many as 20–30% of HRC-I events were being incorrectly located due to electronic saturation in the readout amplifiers and/or A-to-D conversion. With the instrument already in the XRCF chamber, we made the decision to lower the MCP gain until the signals no longer saturated the electronics. For both HRC-I and HRC-S, we lowered the MCP voltages by about 40 volts/plate. This reduced the fraction of events with saturated pulse height to at most a few percent.

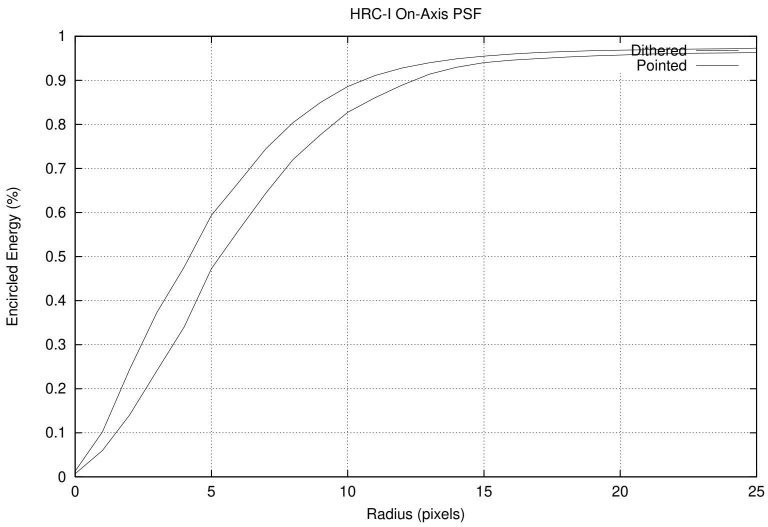

Figure 9. Encircled energy versus radius for dithered and pointed measurements with C-K X-rays

4. XRCF RESULTS

Despite the problems described in the preceding section, the actual XRCF calibration for the HRMA plus HRC started on day 078 (19 March, 1997) and continued through day 102 (12 April, 1997). In that time there were 1111 individual HRC test sequences. The HRC was operated at reduced MCP high voltage and increased event trigger thresholds in order to maintain the very constrained XRCF schedule. Operations were through the same interfaces that will be in place during flight. The data and command formats were identical to flight, although non-flight hardware was used to emulate the configuration. The software systems used to control the instrument, receive and archive the data, and perform realtime display and analysis were the same as those planned for flight. This arrangement gave us a chance to develop and test these interfaces and software. One very positive result was the development of various command sequences for initializing the HRC, and valuable experience in the operational aspect of the detectors.

During the calibration, a huge number of data files are generated. There was a primary instrument data set generated by the HRC EGSE which contains the complete AXAF telemetry stream. From the XRCF X-ray source system there were files that monitor the source. From the SAO Mission Support Team there were files from the various beam monitors used for flux calculations, incident spectra, and spatial uniformity across the telescope aperture. From the Kodak HRMA EGSE there was data on the orientation of the X-ray telescope and the status of grating assemblies. From the Ball FAM EGSE there was data on the location of the instruments in the focal plane. And from the TRW Test Conductor's Log there was a time line of all activities and a listing of the desired parameters for that test. All of these data sources needed to be correlated so that the appropriate information for each test could be extracted. Each data source was time tagged using an IRIG-B time generator, so that this correlation can be made. Unfortunately, during the HRC calibration phase,there were problems with the IRIG system resulting in unreliable time stamps in the data streams. The process of sorting out these inconsistent times has made a complete analysis of the calibration more difficult then expected, and it has delayed some of the results.

None-the-less, a great deal of the calibration has been examined, and preliminary results are available. A few highlights are discussed below, more details are contained in the other HRC papers in this session[1,2].

The overall effective areas for HRC-I and HRC-S are close to that expected values based on the subsystem calibration data and the HRMA model, and generally follow the predicted shapes. The HRC-S appears to have about 20% less efficiency than the HRC-I, which is attributed to the changes in MCP voltage and trigger threshold that were used at the XRCF. More details can be found in the Kenter et al. and Kraft et al. papers from this session[1,2].

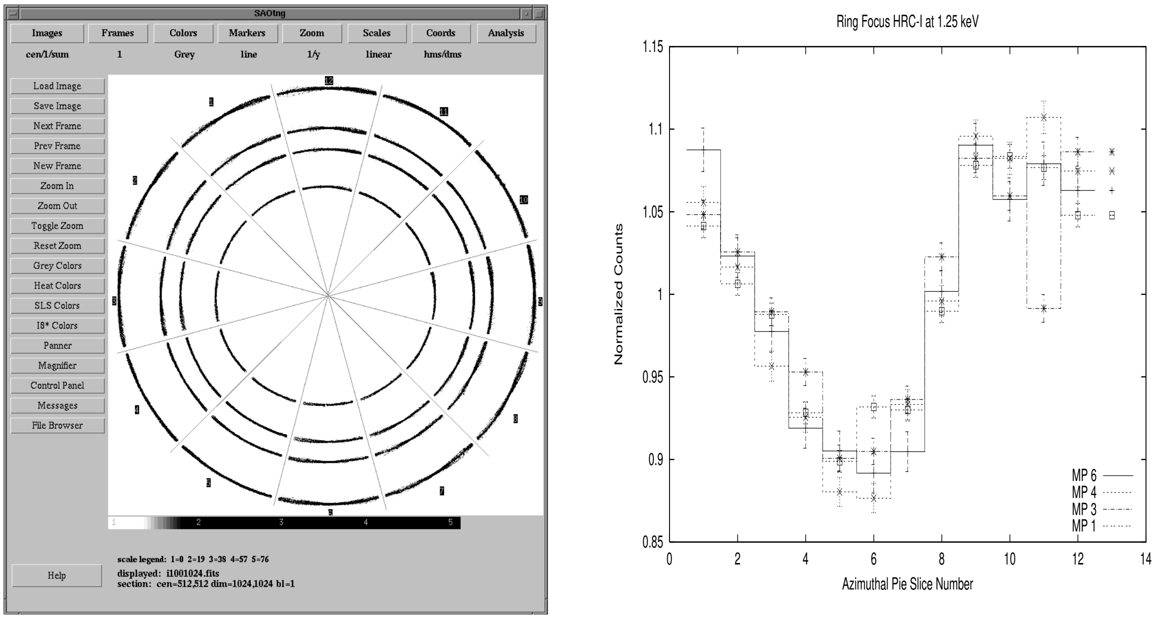

(A) **(B)**

Figure 10. Ring Focus image and the normalized rate versus azimuthal slice for Ring Focus. There is a small azimuthal count dependence of ±10% from the mean. This variation is essentially the same for all four shells, and it is aligned (and consistent) with the direction of the MCP bias angle.

The measured HRMA plus HRC-I point spread function is shown in Figure 9. We find about 50% of the power within a 1 arc-second diameter. A similar measurement that was made without dithering (obtained during the count rate linearity tests) is also shown in Figure 9. This gives a somewhat better PSF indicating that the accuracy of the dither correction is not as good as we expected, or that there are uncorrected motions in the focal plane when dithering.

A long "ring focus" image was made with the HRC-I at 1.25 keV (Mg-K) from which the azimuthal dependence of the HRC quantum efficiency was measured. The AXAF optics generate a cone of X-rays with half angle ranging from about 1.5 to 3.5 degrees relative to the optical axis. The HRC MCPs have a bias angle of about 6 degrees so that some of the X-rays strike the detector at angles as small as 2.5 degrees relative to the MCP pores. Since the MCP quantum efficiency depends on the angle of incidence, there will be a variation of the counting rate around a ring image. Figure 10 shows the results from the ring focus test. The azimuthal variations are within ±10% for all four shells.

5. MODIFICATIONS AND RECALIBRATION

After the XRCF testing was completed the HRC was returned to SAO so that the 91 KHz and high gain problems could be addressed. It was also more convenient to make the flat field measurements at the SAO facilities where a high speed data tap could be used to permit data rates 10 times higher than available at the XRCF.

5.1. Solutions

With the HRC at SAO it was possible to make better diagnostic measurements to help in understanding the root causes of both the 91 KHz ripple seen at MSFC, and also the unexpected higher gain of the analog electronics. The HRC was mounted in a test configuration where there was access to interior test points while the detector housing was held at vacuum allowing the MCPs to be illuminated with X-rays. While diagnosing the HRC problems in this configuration, we carried out a series of flat field measurements for both HRC-S and HRC-I to establish a baseline set of measurements corresponding to the XRCF state of the instrument. Measurements were made at the same

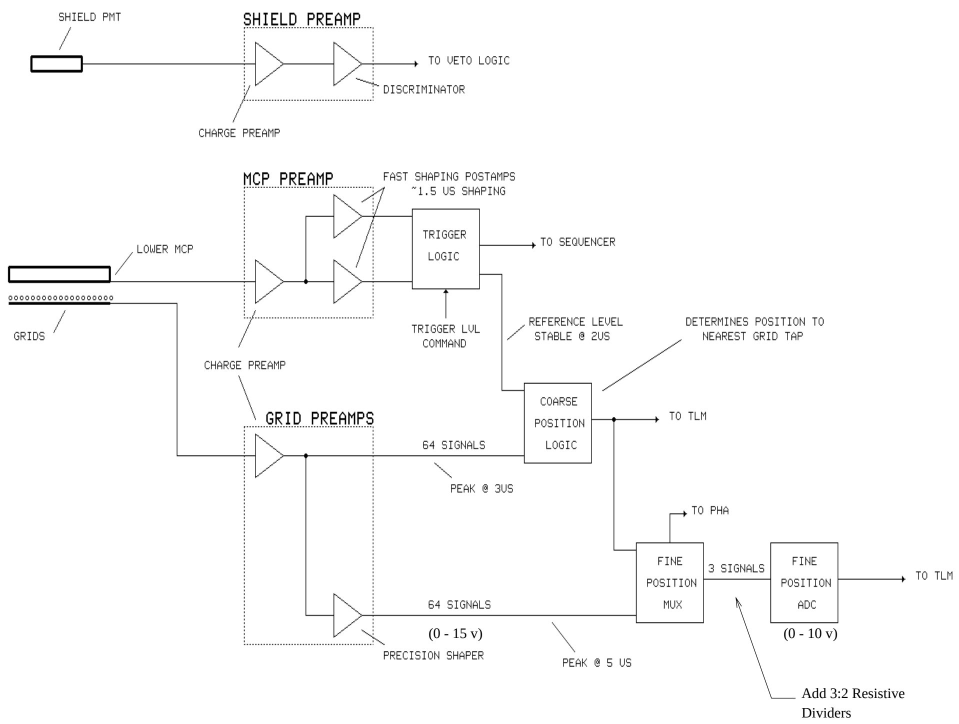

Figure 11. Block diagram of the front end electronics. The hybrid preamps have a linear range of 0 – 15 v, while the subsequent fine position ADC has a 0 – 10 v linear range. By inserting a 3:2 resistive divider at the inputs to the fine position ADC's the extended range of the preampliers will not result in saturation in the ADC.

8 energies as the subassembly calibrations. These measurements (taken at the lower MCP high voltage settings, and increased trigger threshold levels) clearly showed significant energy dependent spatial variations in detection efficiency.

5.1.1. High Gain

The desired electronic gain was determined during the early phase of the instrument development cycle and this value was incorporated into the specifications for the hybrid preamplifier vendor. In retrospect, that gain requirement was probably derived from laboratory tests of MCPs that were either not coated with CsI, or were not of the same type (e.g. low noise) as the flight MCPs. However, this discrepancy was not noted prior to the XRCF tests. Due to the pressing AXAF schedule, the fully assembled HRC was not tested before being shipped to MSFC, so there was no data to suggest a problem.

The front end electronic gain of the HRC is controlled by settings on each of the 128 charge sensitive hybrid preamplifiers (64 per axis). There are two sets of these preamps for a grand total of 256 devices. The gain is controlled by a resistor in the operational amplifier feedback loop of each preamp. The hybrid units are individually trimmed, sealed in hermetic cans, and wave soldered to printed wire circuit boards. Each hybrid preamp PWC holds 8 units, for a total of 16 such boards.

The most direct solution was to modify all of the 256 hybrid preamplifiers; however, the risk would have been much too high. Fortunately an alternative solution was found. In Figure 11 we show a simplified block diagram of the HRC Front End Electronics (FEA). The linear range of the grid hybrid preamps is 50% greater than the linear range of the rest of the analog processing chain. By adding 3:2 resistive dividers at the inputs of the three fine position analog to digital converters (for each axis), the overall electronic gain was decreased by 50% allowing the MCPs to operated at their nominal high voltage (and gain) without producing electronic saturation. These changes were relatively easy to implement.

5.1.2. 91 KHz Ripple

While still at the XRCF, this problem was traced to the R-C filter network between the HVPS and the detector. Due to schedule pressures, the fully assembled HRC instrument was never completely tested prior to shipment to the XRCF. The detector subsystem tests discussed above were all made with non-flight high voltage power supplies and filter networks. At the XRCF, repair or replacement of the filter network was considered and rejected since it involved a major disassembly of the certified clean instrument, and would have meant that the HRC and HRMA could not be calibrated together. (The overall AXAF schedule required the HRMA to be shipped to TRW to begin spacecraft integration by the end of April.)

However, we did begin the work of redesigning the filter network, adding an additional R-C stage to better isolate the DC-DC converter from the MCPs. By the time the HRC was returned to SAO, we had these new filters available for testing and replacement. When the initial flat field tests were completed, the HRC was taken from the X-ray calibration system and placed in a clean room so that the electronics box containing the high voltage power supplies and filter networks could be removed. The disassembly of the unit, was followed by the removal of the faulty filter networks and their replacement.

5.1.3. Recalibration

The re-assembled unit was then placed back in the calibration facility for a additional flat field measurements. Two measurements were made at each test energy. One where only the MCP high voltage was changed relative to the XRCF configuration, and a second where both the high voltage and the trigger level were changed. The high voltage settings were close to the values used during the subsystem level tests, and the event trigger levels were set to 8 DU for both the HRC-I and HRC-S.

Figure 12 shows a flat field surface plot for the HRC-I taken at the three configurations used. The number of counts in a 0.8mm square pixel is plotted versus the U-V position of the pixel. The counts are plotted in arbitrary units where 100 is the the average for the field. Also plotted are contours of constant counts, Panel (A) is status during the XRCF calibration, showing the rapid fall off in detector response around the detector edges. This behavior present at all energies and explains the decrease in HRC-I off-axis efficiency. In panel (B) the MCP high voltage was increased, and there is considerable reduction in the fall off of the detector response. In panel (C), the effect of also lowering the event trigger level is seen. The detector response is much more uniform ($\pm 5\%$ over 95% of the active area). There is also a small increase in the peak absolute efficiency of the HRC-I in this final operating configuration.

Figure 13 is a surface plot for the +1 segment of the HRC-S. This is the segment along the +Y axis of AXAF and was the section of the HRC-S that showed greatest spatial non-uniformity during the XRCF. The number of counts in 0.8mm pixels (normalized to arbitrary units) is plotted versus the U-V pixel coordinates. The leftmost plot (A) is for the XRCF operating conditions. Variations in the detector efficiency are as large as 50% along the V (dispersion) direction. The center plot (B) shows the effects of increasing the MCP high voltage. The plot shows much less variation than for the XRCF configuration. At the same time, the absolute efficiency at this voltage is almost 40% higher than the previous configuration. This improvement results from driving more of the MCP area into saturation at the higher operating voltage. Finally the rightmost plot (C) shows the effect of also decreasing the trigger threshold level after removing the 91 KHz feedthrough. The response is much more uniform along the V-axis, variations are only about $\pm 10\%$, and the U-axis variations have also decreased. With these modifications, all three HRC-S segments now show similar behavior. The left-right asymmetry seen during the XRCF has been greatly reduced, and the absolute detection efficiency is close to the subsystem values obtained prior to the XRCF tests.

6. CONCLUSIONS

The HRC has been fully calibrated and recalibrated using the facilities at SAO and the XRCF at MSFC. Two problems were discovered during the XRCF phase of calibration and these were corrected during rework at SAO. The instrument (which is presently being integrated onto the AXAF Science Instrument Module) now meets or exceeds all of the performance specifications.

Some valuable lessons have been learned in this process, key of which is the need to adequately test an instrument in its final configuration, and to be able to analyze calibration data in as near to real-time as possible.

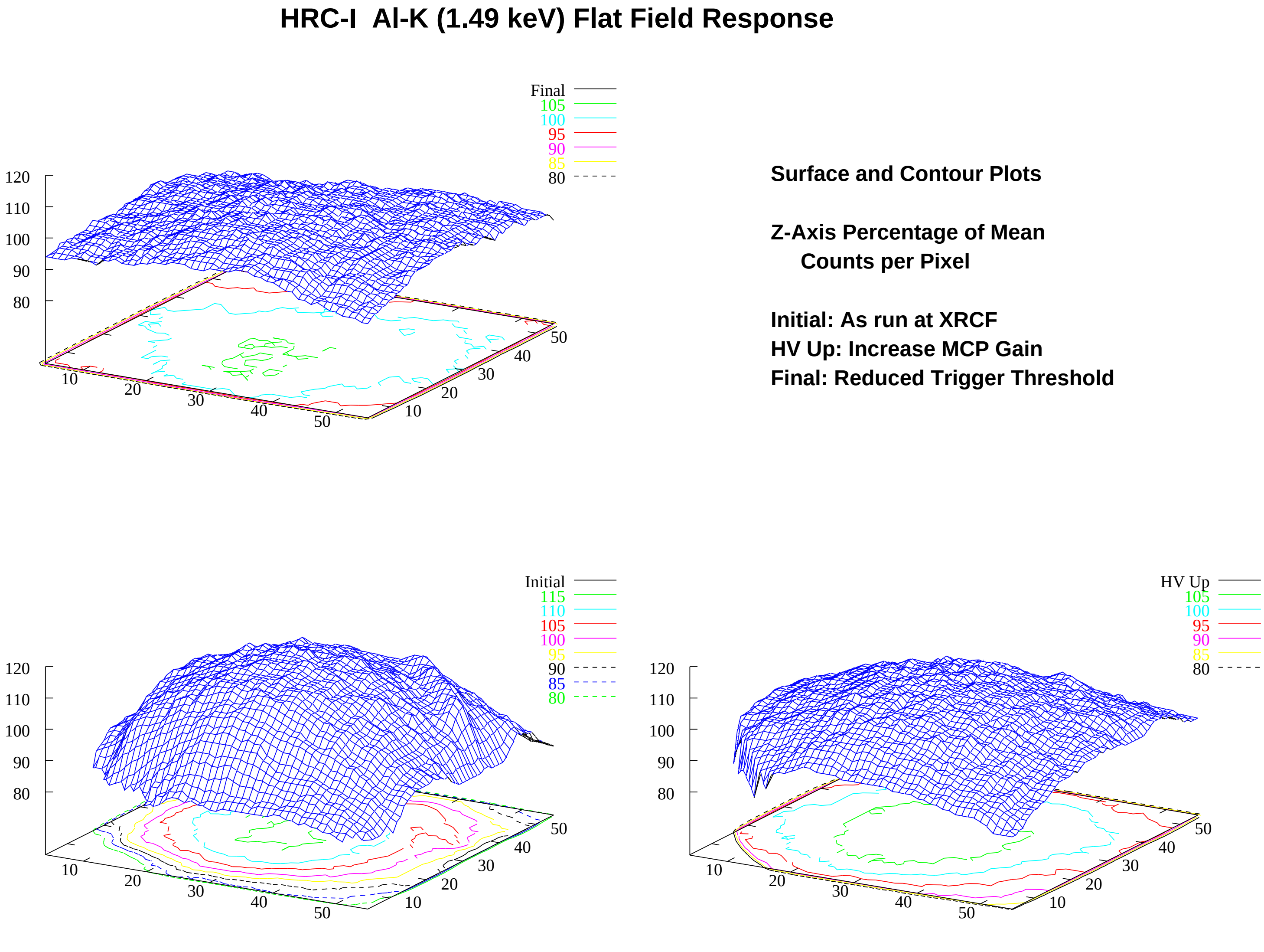

Figure 12. Surface plots of an HRC-I flat field measurement at Al-K (1.49 keV).

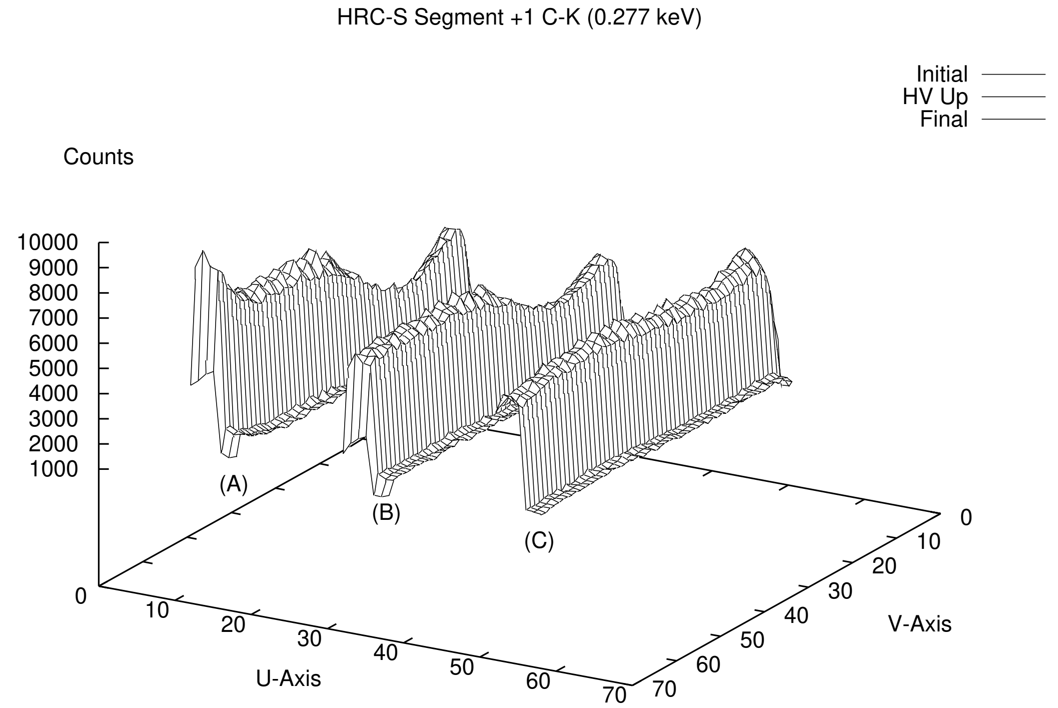

Figure 13. Surface plots of an HRC-S flat field measurement at C-K. The +1 segment of the spectroscopy detector is shown

ACKNOWLEDGEMENTS

The authors would like to thank Mr. Gerald Austin for his tireless efforts in the construction and testing of the HRC. We also thank Jack Gomes, John Polizotti, Everett Johnston, Adrian Roy and Richard Goddard for their outstanding engineering support. The HRC was designed and built at SAO, and we thank all the Central Engineering staff for their contributions.

This work has been supported by NASA contract NAS8-38248.

REFERENCES

1. Kenter, A.T., Chappell, J.H, Kobayashi, K., Kraft, R.P., Meehan, G.R., Murray, S.S., Zombeck, M.V., Smithsonian Astrophysical Observatory; Fraser, G.W., Pearson, J.F., Lees, J.E., Brunton, A.N., Pearce, S.E., University of Leicester (UK); Barbera, M., Collura, A., Serio, S., Instituto e Osservatorio Astronomico G.S. Vaiana (Italy) "Performance and Calibration of the AXAF High Resolution Camera I: Imaging Readout", SPIE **3114**, (1997).
2. Kraft, R.P., Chappell, J.H, Kenter, A.T., Kobayashi, K., Meehan, G.R., Murray, S.S., Zombeck, M.V., Smithsonian Astrophysical Observatory; Fraser, G.W., Pearson, J.F., Lees, J.E., Brunton, A.N., Pearce, S.E., University of Leicester (UK); Barbera, M., Collura, A., Serio, S., Instituto e Osservatorio Astronomico G.S. Vaiana (Italy) "Performance and Calibration of the AXAF High Resolution Camera II: Spectroscopic Detector", SPIE **3114**, (1997).
3. Meehan, G.R., Murray, S.S., Zombeck, M.V., Kraft, R.P., Kobayashi, K., Chappell, J.H, Kenter, A.T., Smithsonian Astrophysical Observatory; Fraser, G.W., Pearson, J.F., Lees, J.E., Brunton, A.N., Pearce, S.E., University of Leicester (UK); Barbera, M., Collura, A., Serio, S., Instituto e Osservatorio Astronomico G.S. Vaiana (Italy) "Calibration of the UV/Ion Shields for the AXAF High Resolution Camera", SPIE **3114**, (1997).

4. M.V. Zombeck, J.H. Chappell, A. Kenter, R.W. Moore, S.S. Murray, "The High Resolution Camera (HRC) on the Advanced X-ray Astrophysics Facility (AXAF)," Proc. SPIE, 2518, 1996
5. Markert, T.H., Canizares, C.R., Dewey, D., McGuirk, M., Pak, C.S., Schattenburg, M.L., "High Energy Transmission Grating Spectrometer (HETGS) for AXAF", in *EUV, X-Ray, and Gamma-Ray Instrumentation for Astronomy V*, SPIE **2280**,(1994).
6. P. Predehl, H. Kraus, H. W. Bruninger, W. Burkert, G. Kettenrin und H. Lochbihler, "Grating elements for the low energy transmission grating spectrometer for AXAF", Proc. SPIE 1743, 475-481 (1992).
7. Meehan, G.R., Chappell, J.H, Kenter, A.T., Kraft, R.P., Kobayashi, K., Murray, S.S., Zombeck, M.V., Barbera, M, Collura, A. "Measurement of the Transmission of the UV ion Shields of the AXAF High Resolution Camera", SPIE **2808**, (1996).